

Hydrogen Diffusion in Magnesium Using Machine Learning Potentials

Andrea Angeletti^{1,*}, Luca Leoni^{2,+}, Dario Massa^{3,+}, Luca Pasquini², Stefanos Papanikolaou³, and Cesare Franchini^{1,2}

¹University of Vienna, Vienna Doctoral School in Physics, Boltzmannngasse 5, 1090, Vienna, Austria, Europe

²Department of Physics and Astronomy 'Augusto Righi', Alma Mater Studiorum - Università di Bologna, Viale Berti Pichat 6/2, 40127, Bologna, Italy, Europe

³NOMATEN Centre of Excellence, National Center for Nuclear Research, 05-400, Otwock, Poland, Europe

*Corresponding author: andrea.angeletti@univie.ac.at

+These authors contributed equally to this work

ABSTRACT

Understanding and accurately predicting hydrogen diffusion in materials is challenging due to the complex interactions between hydrogen defects and the crystal lattice. These interactions span large length and time scales, making them difficult to address with standard ab initio techniques. This work addresses this challenge by employing accelerated machine learning (ML) molecular dynamics simulations through active learning. We conduct a comparative study of different ML-based interatomic potential schemes, including VASP, MACE, and CHGNet, utilizing various training strategies such as on-the-fly learning, pre-trained universal models, and fine-tuning. We obtain an optimal hydrogen diffusion coefficient value of $2.1 \cdot 10^{-8} \text{ m}^2/\text{s}$ at 673 K in $\text{MgH}_{0.06}$, which aligns exceptionally well with experimental results, underlining the efficacy and accuracy of ML-assisted methodologies in the context of diffusive dynamics. Particularly, our procedure significantly reduces the computational effort associated with traditional transition state calculations or ad-hoc designed interatomic potentials. The results highlight the limitations of pre-trained universal solutions for defective materials and how they can be improved by fine-tuning. Specifically, fine-tuning the models on a database produced during on-the-fly training of VASP ML force field allows the retrieving of DFT-level accuracy at a fraction of the computational cost.

1 Introduction

The global imperative for sustainable and green energy solutions has intensified the search for efficient hydrogen storage materials. With the highest energy density among fuels¹, hydrogen represents a promising alternative to fossil sources that can be produced with zero CO_2 emissions powered by surplus renewable energy², through methods such as electrolysis³⁻⁵. The main barrier preventing a future economy based on hydrogen energy is the absence of a green, safe and efficient way to store and transport it. Solid state hydrogen storage technologies are the most studied in this regard, being the safest, offering higher volumetric densities⁶ than cryogenic or high-pressure gaseous alternatives⁷⁻⁹. Despite these advantages, the technology remains in its early stages and the search for materials allowing large-scale applications, like in the automotive industry¹⁰, remains open^{11,12}.

Among promising candidates, magnesium stands out for its excellent hydrogen storage capacity¹³, environmental friendliness, and natural abundance, displaying theoretical storage capacities as high as 7.6% wt¹⁴. However, the slow kinetics of hydrogen in magnesium-based compounds still pose a limit to possible applications. Therefore, understanding and optimizing hydrogen diffusion pathways through theoretical modeling¹⁵⁻¹⁷ and experimental studies¹⁸⁻²⁰ is crucial in order to improve performances of future Mg-based hydrogen storage materials. Despite numerous efforts over the past decade, modeling hydrogen dynamics in solid-state compounds remains challenging²¹⁻²⁴. The low hydrogen diffusivity in magnesium requires prolonged simulation times, in the order of nanoseconds, for accurate studies using ab-initio Molecular Dynamics (MD). Consequently, ab-initio transition state calculations, such as the nudged elastic band (NEB) method, have emerged as the most effective approaches to reproduce and interpret the experimental data documented in the literature to date¹⁶. However, this technique is cumbersome and often impracticable for systems with high defect concentrations, or complex potential energy landscapes: manually describing all possible paths required by NEB may be very challenging and virtually impossible¹⁶.

Recently, Machine Learning accelerated MD (MLMD) has revolutionized the world of MD by making accurate simulations of large systems accessible over long time scales²⁵. The application of such approach to study hydrogen defective systems is of high interest²⁶, since the prediction of dynamical properties would highly expand the limited landscape offered by today transition state computations. MLMD does allow the study of multi-component system²⁷ and can efficiently account for

interaction between defects²⁸. However, developing accurate interatomic potentials, especially for hydrogen-defective materials, is notoriously challenging^{29,30}. Still, the field is rapidly growing and several new approaches were proposed to explore new and complex phase spaces. On one side, various pre-trained universal solutions^{31,32} start to be available, aiming to offer a convenient and versatile way tackling the problem. However, as discussed in this work, while their training datasets are rich in chemical compositional space, the limited configurational sampling can significantly compromise their accuracy on previously unseen defected, metastable and transition states, leading to ungranted generalization capabilities. On the other side, active-learning approaches based on Bayesian force fields are showing a large versatility thanks to the construction of on-the-fly databases^{33,34}. The error-oriented sampling of configurations allows these models to easily collect high-quality data widely spanning the configurational space, thus making them highly accurate despite their architecture, constrained compared to neural networks. The current study aims at illustrating a systematic procedure for ML-potentials applications in diffusive dynamics conditions, which can be used to enhance the study of different embedded defects, without departing from ab-initio accuracy. This procedure specifically consists in improving ML-based pre-trained models' performance via actively learned configurations, generated by on-the-fly training of the Vienna Ab Initio Simulation Package Bayesian ML Force-Field (VASP-MLFF)^{33,34}. Particularly, we focus our attention on $\text{MgH}_{0.06}$, computing the Hydrogen diffusion coefficient at different temperatures, employing a proper methodology which ensures accurate analysis of unbiased dynamical properties. Two different Universal Interatomic Potentials (UIPs), CHGNet³¹ and MACE³², were considered. Dynamical properties were computed for VASP-MLFF alongside the pre-trained and fine-tuned versions of the UIPs. The comparison between the different results and experimental data showed excellent agreement, both with VASP-MLFF and fine-tuned potentials, while their pre-trained versions fails to reach a satisfactory accuracy. Interestingly, the fine-tuned potentials outperform VASP-MLFF by correctly predicting the temperature dependence of the diffusion coefficient.

2 Material and Methods

2.1 MLFF-MD

The Density Functional Theory (DFT) and MLFF MD calculations were performed using VASP^{35,36}. For the molecular dynamics simulations, we utilized a $4 \times 4 \times 4$ supercell, shown in Fig. 1, comprising of 128 Mg atoms in hcp crystal symmetry, with 8 H atoms randomly distributed in the lattice. All the computations were performed at the Perdew-Burke-Ernzerhof (PBE) functional level of theory³⁷, using an energy cutoff of 600 eV with a convergence threshold of 0.1 meV. The temperature was incrementally raised from 0 to 700 K over a 0.2 ns interval with VASP on-the-fly MLFF-MD. In this setup, derived configurations—including structure energy, forces acting on each atom, atomic coordinates, stress tensor, and lattice parameters—were used to train the interatomic potential. Whenever the Bayesian error surpassed the set fixed threshold, VASP reverted to DFT to generate a new configuration in the database. Such on-the-fly procedure allows the model to use the accumulated ab-initio configurations to gradually improve the predictions on subsequent steps. The threshold value of

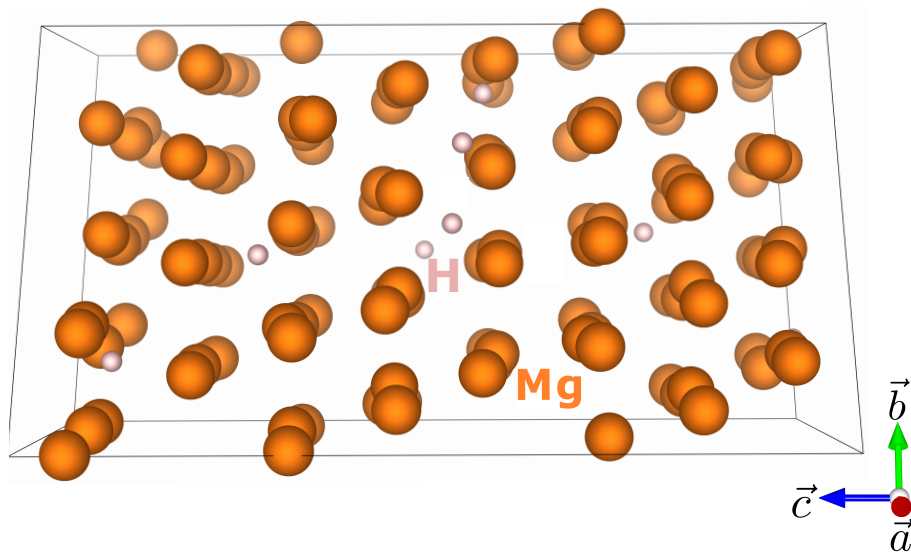


Figure 1. Perspective view of a MLFF-MD frame, at 673 K, of the $4 \times 4 \times 4$ $\text{MgH}_{0.06}$ supercell employed in the calculations, (Mg atoms in orange and H atoms in pink).

5 meV/Å has been set to ensure a collection of diverse and well-spread representation of structures in the database from the explored configurational phase space. During the thermalization phase, we opted for an NpT ensemble while constraining the cell shape, employing the Langevin thermostat with a friction coefficient for the lattice and atomic degrees-of-freedom equal to 10 ps^{-1} . We applied zero external pressure and with a time step of 1 fs. At key temperatures of 300 K, 480 K and 673 K, we conducted further 100 ps long NpT simulations in training mode to accumulate additional configurations. A total of over 3,700 ab-initio configurations have been stored, fewer than 1,000 being recorded at each constant temperature, and the remaining configurations captured during the ramping phase. Subsequently, we switched to MLFF-MD in run mode and determined the average lattice volume over a 100 ps period at fixed temperatures of 300 K, 480 K, and 670 K. The average volume configurations were then utilized to conduct NVT simulations. Following a 100 ps NVT simulation, we extracted the average energy configurations for use in subsequent NVE simulations, where we computed the mean squared displacements (MSD) of hydrogen atoms as the ensemble average of

$$\text{MSD}(t) = \frac{1}{T-t} \int_0^{T-t} [\mathbf{r}(t+\Delta) - \mathbf{r}(\Delta)]^2 d\Delta. \quad (1)$$

Where T is the total simulation time, and \mathbf{r} is the trajectory of the atoms under analysis. All the MSD were constructed over NVE trajectories of at least 1 ns, and used to extract the diffusion coefficient D by fitting the linear part of the function with the Einstein relation

$$\text{MSD}(t) = 6Dt \quad (2)$$

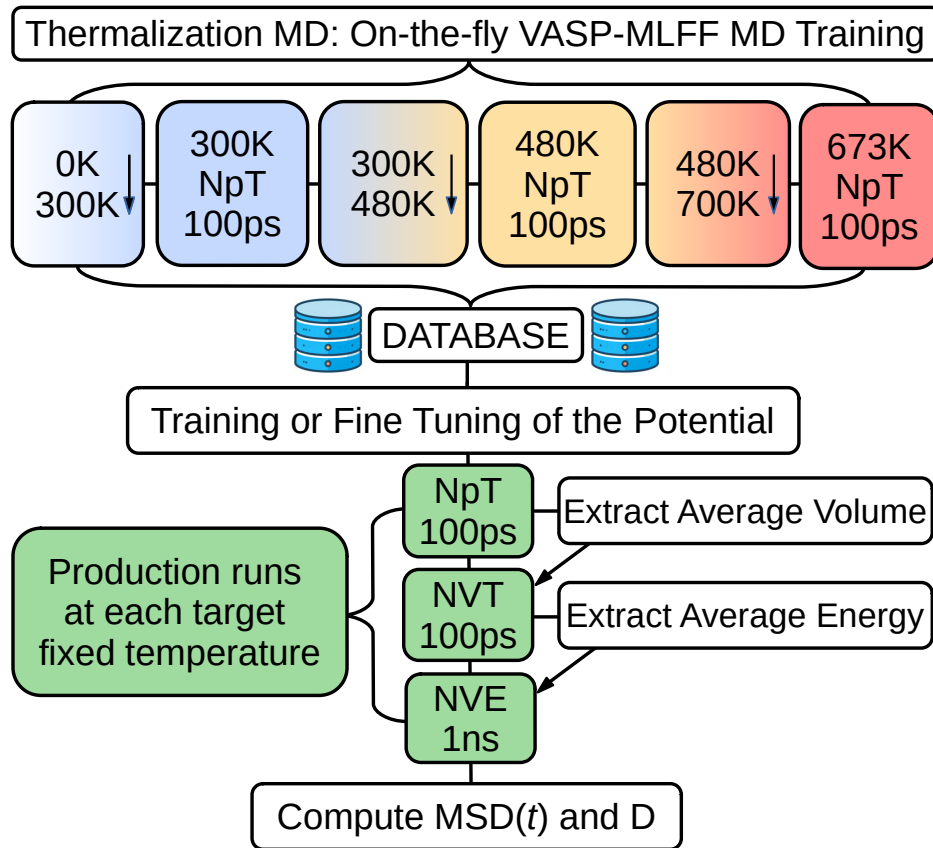


Figure 2. Methodological protocol employed to improve the performance of interatomic potentials and obtain dynamical properties. The database of configurations is built both during NpT-MD thermalizations of the system from 0 K to 700 K via active learning of the VASP-MLFF, and at target temperatures (300 K, 480 K and 673 K). Subsequently, the machine learned potentials are fine tuned or trained, and after system-equilibration the MSD and the diffusion coefficient D at fixed T are computed.

2.2 Universal inter-atomic potentials UIPs

We consider two state-of-the-art best performing³⁸ pre-trained UIPs: MACE³⁹, based on an equivariant message passing neural network, and CHGNET³¹, a graph-based neural network. The models are imported in their pre-trained versions on the Materials Project (MP) relaxation trajectories database⁴⁰, comprising 1.6 millions crystal structures with the associated energies, forces, stresses and magnetic moments. In order to tackle the predicted dynamical properties from such UIPs, we followed the same MD procedure (excluding the on-the-fly training phase) as explained in the previous section. Subsequently, CHGNet and MACE were fine-tuned on the VASP-DFT generated data obtained during the on-the-fly MLFF-MD. MACE was also trained from scratch on the dataset. Regarding CHGNet, it was difficult to stabilize the temperature during the NVE run with 1 fs time step while we observed no drift using 0.5 fs time step. To perform the MD simulations we employed LAMMPS⁴¹ and ASE⁴², for MACE and CHGNet respectively. A schematic view of the employed workflow is represented in Figure (2).

3 Results and Discussions

To assess the performances of every model used in this study, we evaluated the Root Mean Square Errors (RMSE) for the prediction of energy and forces, over a test dataset of 1000 configurations randomly sampled during the NVE run of the VASP-MLFF model. The results reported in Fig. (3) show how the predictions of the VASP-MLFF reach an accuracy of 0.3 meV/atom for energies and 40 meV/Å for forces, respectively, as reasonably expected compared to other studies involving MLFF-MD^{43–46}. On the other hand, the UIPs pre-trained on the MP-database, respectively named on CHGNet_MP and MACE_MP, failed to reach such level of accuracy by more than one order of magnitude. The discrepancy was significantly reduced after fine-tuning the two models on the VASP-generated database: the error obtained shows that the CHGNet_FT performance reaches a level comparable with the VASP-MLFF, and MACE_FT even outperforms it. The corresponding parity plot for CHGNet_MP and CHGNet_FT are displayed in Supplementary Figure 1. The performance differences between CHGNet_FT (1.1 meV/atom) and MACE_FT (0.3 meV/atom), may stem from the equivariant architecture employed by the latter. MACE turned out to be highly data-efficient, leading to better fine-tuning results over small datasets, compared to the more data-hungry architectures like CHGNet. The MACE model was also trained from scratch on the VASP-DFT configurations (MACE_TR), achieving slightly smaller errors on forces with respect to MACE_FT.

The diffusion coefficient predicted from every model during the NVE runs is reported in Fig. (4), and compared with experimental¹⁸ and NEB¹⁶ results, at each investigated temperature. The results clearly show that our procedure provides multiple solutions with excellent experimental agreement, outperforming NEB computations that until now represented the

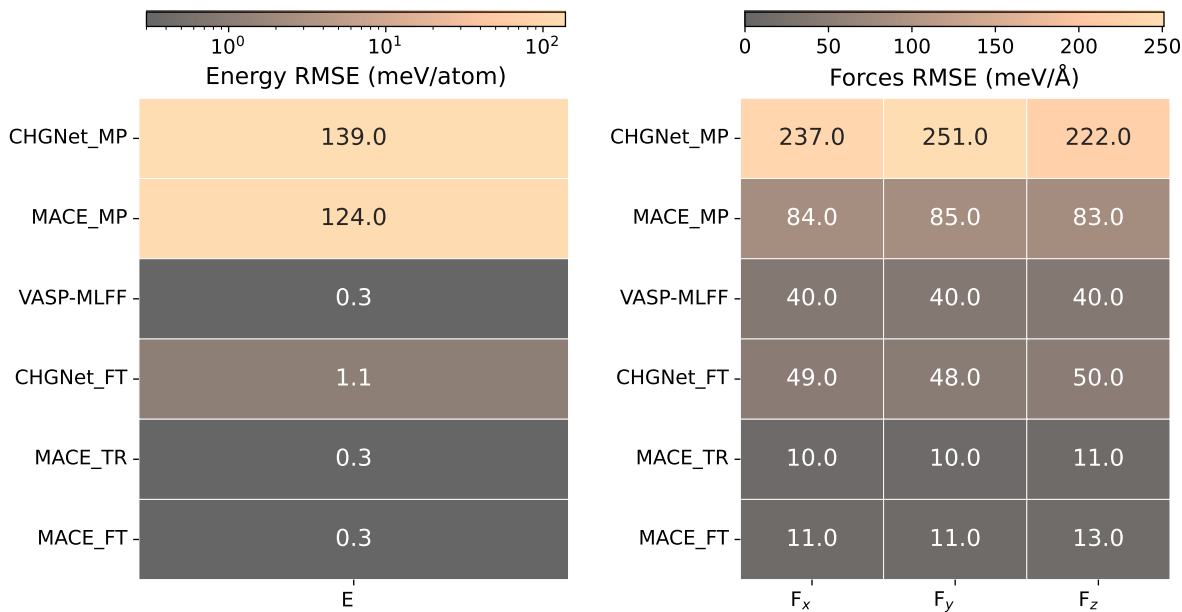


Figure 3. RMSE values for the predictions of energies (E) and forces (F_x, F_y, F_z) on the validation set from every model considered in the study. It can be seen how the finetuning of the foundation models is needed to achieve an error comparable to the MLFF one. The subscript 'MP' refers to the pre-trained model on the Material Project database, 'TR' to the one trained from scratch and 'FT' to the fine-tuned version.

standard for such applications. This holds true for the MACE_FT potential in particular, which not only predicts the correct order of magnitude across all temperatures, but significantly agrees both at 300 K and 673 K. The VASP-MLFF instead, shows a remarkable agreement at 480 K and 673 K, while missing the room temperature by one order of magnitude. For what concerns CHGNet_FT, it provides agreement with the experimental value at 480 K, but at the lowest and highest temperatures respectively overestimates and underestimates the result by one order of magnitude. As expected from the error analysis on energies and forces, both the pre-trained versions of the UIPs result in much lower agreement, with deviations of at least one order of magnitude from experimental values at most temperatures.

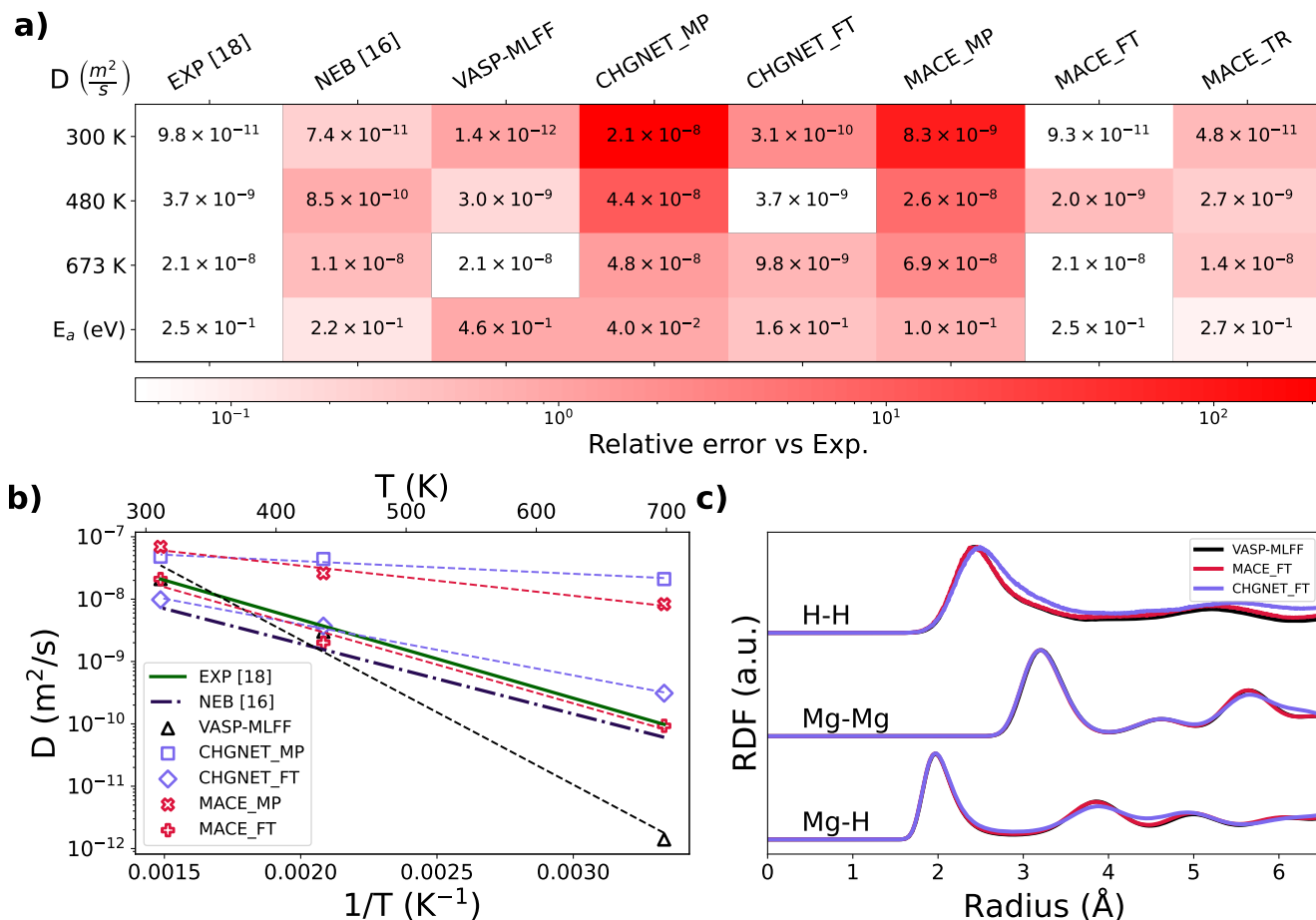


Figure 4. a) Diffusion coefficient values of hydrogen in $MgH_{0.06}$ at three different constant average temperatures of 380 K, 480 K and 673 K, and the corresponding activation energy barrier, showing the comparison of the results achieved via different potentials in our investigations and previous studies. The colorbar highlights in logscale the relative deviation with respect to the experimental values. The linear region of the fit performed on the $MSD(t)$ is reported in Supplementary Figure 2. b) Comparison between the dependence of the diffusion coefficient with temperature, for VASP-MLFF, the fine-tuned UIPs, the NEB and experimental results. c) Radial distribution function of atoms pairs at 673 K during 1 ns long NVE simulations. It is possible to see how the VASP-MLFF and MACE show a remarkable agreement over the whole domain for every pair, while CHGNet starts to differ at larger distances.

A closer inspection of the temperature dependence of the diffusion coefficients, as shown in Fig. (4), reveals that CHGNet_FT still outperforms the VASP-MLFF by better reproducing the Arrhenius curve observed in the experiments, while the MACE_FT solutions outperform both. This shows how with smaller errors, the deep networks are capable to better represent the shape of the energy landscape, with respect to the Bayesian alternative.

In this regard, further quantitative analysis can be provided by comparing the predicted value of the energy barrier, obtained from the linear fits in the Arrhenius plots. In particular, we achieved values of 0.46 eV for VASP-MLFF, 0.16 for CHGNet_FT and 0.25 eV for MACE_FT, where the experiment value corresponds to 0.25 eV¹⁸. MACE_FT clearly excels at representing the

energy landscape of the system, achieving a final barrier value within 1% error of the experimental value, as shown in Fig. (4a). Further analysis have been performed on the dynamics of the system by evaluating the radial distribution function (RDF) in all of the NVE run performed. We report in Fig. (4c) the predicted behaviour by the best performing models in the system at 673 K, while other temperature cases can be found in the SI. A very good agreement between MACE_FT and VASP-MLFF is found, while the RDF of CHGNet_FT departs from the others at larger distances, by smoothing out peaks. From such curves it is possible to retain information about the behaviour of Hydrogen during the simulation. Proceeding in order with increasing distance radius, the first peak appears just before 2 Å in the Mg-H curve, in correspondence of the average distance of one Magnesium atom from the center of the nearest octahedral sites on which Hydrogen tend to sit¹⁵. The second peak, belonging to the H-H pair, is very pronounced at around 2.6 Å, reflecting a correlation between hydrogen atoms at this distance. This behaviour finds agreement in the literature for molecular dynamics with magnesium hydride nanoclusters²⁹. As reported in Fig (6), on average we found that there are always at least two hydrogen pairs below a distance of 3 Å. In fact, the distance of 2.6 Å corresponds to the one between two octahedral sites along the c-direction¹⁵, as also reported in literature²⁹, implying how Hydrogen tend to sit on near sites. To highlight such behaviour we also report in Fig. (5) the extensive diffusion path of a representative hydrogen atom within the magnesium matrix during a 100 ps simulation, at 673 K. The trajectory is unwrapped in the replicas of the periodic images to enhance visibility and interpretation. The color gradient serves as a temporal marker, with blue indicating the initial position of the hydrogen atom at the beginning of the simulation (t = 0 ps) and red indicating its position at the end of the studied interval (t = 100 ps). Intermediate colors (cyan, green, yellow, and orange) represent the progression of time between these two extremes, providing a visual cue for the temporal evolution of the atom's diffusion path. The black circles highlight interstitial regions where the hydrogen atom tends to oscillate around the magnesium sites, indicating temporary trapping sites within the lattice structure, before continuing its diffusion trajectory. The third significant peak in the RDF is observed around 3 Å in the Mg-Mg curve, consistently with the typical magnesium distances in hcp structures. Multiple smaller peaks indicate further neighbor interactions in the crystal lattice. Analogous results were found in the RDF at 300 K and 480 K, where the peaks are sharper due to the reduced effect of thermal motion, see Supplementary Figure 3. In particular, higher pronounced RDF at lower temperature indicates that hydrogen tend to spend more time in the vicinity of Magnesium, and diffuse less in the crystal structure.

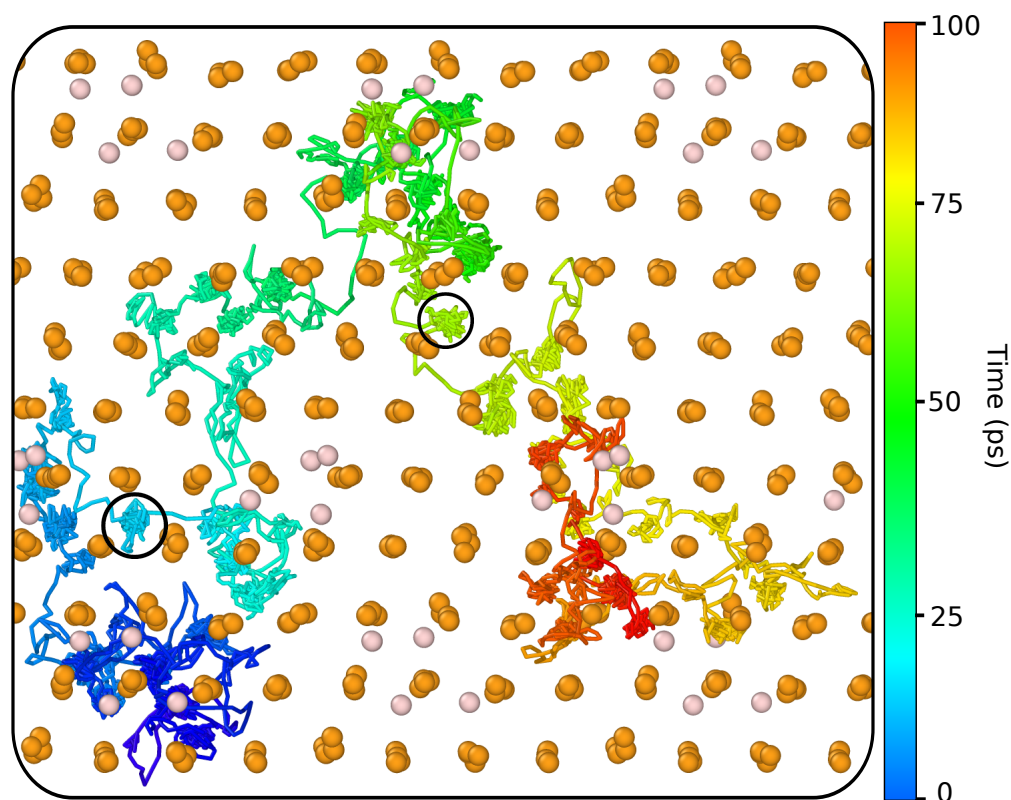


Figure 5. Diffusion path of a representative hydrogen atom during 100 ps at 673K, within the magnesium bulk, depicted using a color-gradient line to represent the progression of time, from blue to red. The black circles highlight the interstitial regions where H atoms tend to oscillate around Mg lattice site before continuing their diffusing trajectory.

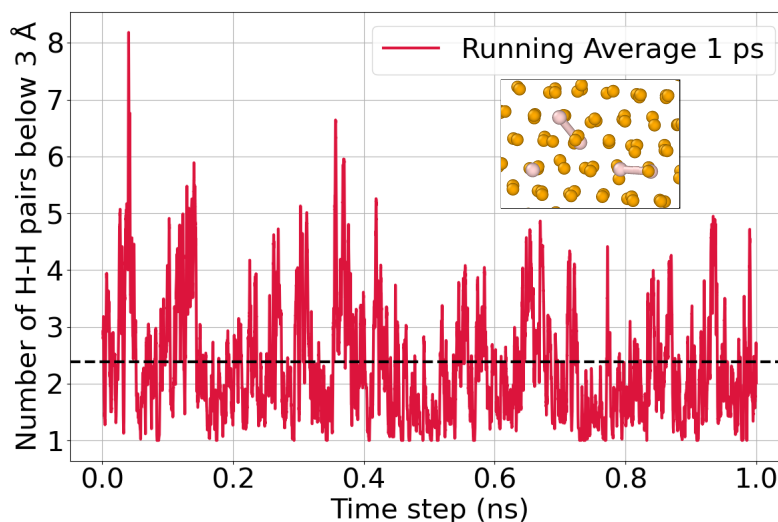


Figure 6. Number of hydrogen pairs below a threshold distance of 3 Å averaged over 1 ps (in red), and the average value over the entire simulation (black dashed line).

4 Conclusion

Our investigation enabled to thoroughly characterize the kinetic properties and mobility of hydrogen within a structured environment, such as pure magnesium, across various temperatures, through a rigorous and efficient methodology. We performed a systematic and comparative study of ML-based interatomic potential MD schemes, particularly focusing on Bayesian versus equivariant and graph neural networks (MACE and CHGNet), under different training modes (universal and fine-tuned). The results were validated by estimates of the diffusion coefficient values, which showed excellent agreement with experimental data. The obtained results proved that the VASP-DFT configurations, collected during the MLFF on-the-fly training, represent a complete set for the accurate modeling of inter-atomic interactions, between hydrogen and magnesium atoms. This strategy could be consistently applied to generate a comprehensive dataset for the proper training of existing or forthcoming potentials. In fact, we identified the limitations of pretrained UIPs in studying materials with diffusing defects, due to the absence of representative high temperatures, defective and metastable states in their datasets. Particularly, we demonstrated the ability of state-of-the-art machine learning models to achieve DFT-level accuracy, after fine-tuning on actively learned DFT-configurations, highlighting the importance of focusing on efficient dataset-building methods and their quality. Specifically, the importance of including defected and transition-state configurations, as well as the role of transfer-learning, allowing pre-trained solutions to adapt to new systems. These progresses not only improve our understanding of hydrogen interactions in magnesium, but also pave the way for future research into a broader range of multi-component systems and defected compositions. This is especially significant for systems with complex potential energy surfaces, where traditional ab-initio methods become impractical. Successfully modeling the hydrogen diffusion mechanism in magnesium via machine learning-accelerated molecular dynamics could facilitate the study and discovery of new, more efficient materials for hydrogen storage and beyond it, contributing to the transition towards a greener and more sustainable energy future.

Acknowledgments

C. F. and A. A. acknowledges the "Doctoral College Advanced Functional Materials – Hierarchical Design of Hybrid Systems DOC 85 doc.funds" funded by the Austrian Science Fund (FWF) and by the Vienna Doctoral School in Physics (VDSP). For Open Access purposes, the author has applied a CC BY public copyright license to any author accepted manuscript version arising from this submission. D. M. and S. P. were supported by the European Union Horizon 2020 research and innovation program under Grant Agreement No. 857470, from the European Regional Development Fund under the program of the Foundation for Polish Science International Research Agenda PLUS, grant No. MAB PLUS/2018/8, and the initiative of the Ministry of Science and Higher Education 'Support for the activities of Centers of Excellence established in Poland under the Horizon 2020 program' under agreement No. MEiN/2023/DIR/3795. L.P. and C.F. acknowledges the National Recovery and Resilience Plan (NRRP), Mission 4 Component 2 Investment 1.3 - Project NEST (Network 4 Energy Sustainable Transition) of Ministero dell'Università e della Ricerca (MUR), funded by the European Union – NextGenerationEU. L.L. and C.F. acknowledges the NRRP, CN-HPC grant no. (CUP) J33C22001170001, SPOKE 7, of MUR, funded by the European Union – NextGenerationEU. The computational results were obtained using the Vienna Scientific Cluster (VSC) and the LEONARDO cluster through the IS CRA initiative.

Supplementary material

Supplementary information and figures are available at website...

Author Contribution

Conceptualisation: C.F., A. A., D. M. and L. L. Methodology and calculations: A. A., D. M. and L. L. Supervision: C.F. Writing: A.A , D.M. , L. L. and C. F. Discussion and reviewing: All authors

Competing Interests

The authors declare no competing interests.

References

1. Yang, J., Sudik, A., Wolverton, C. & Siegel, D. J. High capacity hydrogen storage materials: Attributes for automotive applications and techniques for materials discovery. *Chem. Soc. Rev.* **39**, 656 – 675 (2010).
2. Bhimineni, S. H. *et al.* Machine-learning-assisted investigation of the diffusion of hydrogen in brine by performing molecular dynamics simulation. *Ind. & Eng. Chem. Res.* **62**, 21385–21396, DOI: [10.1021/acs.iecr.3c01957](https://doi.org/10.1021/acs.iecr.3c01957) (2023). <https://doi.org/10.1021/acs.iecr.3c01957>.
3. Tarasov, B. P. *et al.* Metal hydride hydrogen storage and compression systems for energy storage technologies. *Int. J. Hydrog. Energy* **46**, 13647–13657 (2021).
4. Turner, J. A. A realizable renewable energy future. *Science* **285**, 687 – 689 (1999).
5. Hydrogen production from renewables. *Renew. Energy Focus.* **9**, 34–37 (2009).
6. Aceves, S. M., Berry, G. D., Martinez-Frias, J. & Espinosa-Loza, F. Vehicular storage of hydrogen in insulated pressure vessels. *Int. J. Hydrog. Energy* **31**, 2274–2283 (2006).
7. Sun, Y. *et al.* Tailoring magnesium based materials for hydrogen storage through synthesis: Current state of the art. *Energy Storage Mater.* **10**, 168–198, DOI: <https://doi.org/10.1016/j.ensm.2017.01.010> (2018).
8. Felderhoff, M., Weidenthaler, C., von Helmolt, R. & Eberle, U. Hydrogen storage: the remaining scientific and technological challenges. *Phys. Chem. Chem. Phys.* **9**, 2643–2653 (2007).
9. Hua, T. *et al.* Technical assessment of compressed hydrogen storage tank systems for automotive applications. *Int. J. Hydrog. Energy* **36**, 3037–3049 (2011).
10. US Department of Energy. Doe technical targets for onboard hydrogen storage for light-duty vehicles.
11. Yartys, V. *et al.* Magnesium based materials for hydrogen based energy storage: Past, present and future. *Int. J. Hydrog. Energy* **44**, 7809–7859, DOI: <https://doi.org/10.1016/j.ijhydene.2018.12.212> (2019). A special issue on hydrogen-based Energy storage.
12. Hirscher, M. *et al.* Materials for hydrogen-based energy storage – past, recent progress and future outlook. *J. Alloy. Compd.* **827**, 153548, DOI: <https://doi.org/10.1016/j.jallcom.2019.153548> (2020).

13. Allendorf, M. D. *et al.* Challenges to developing materials for the transport and storage of hydrogen. *Nat. Chem.* **14**, 1214–1223, DOI: [10.1038/s41557-022-01056-2](https://doi.org/10.1038/s41557-022-01056-2) (2022).
14. Gupta, A. & Faisal, M. Magnesium based multi-metallic hybrids with soot for hydrogen storage. *Int. J. Hydrog. Energy* **53**, 93–104, DOI: <https://doi.org/10.1016/j.ijhydene.2023.12.020> (2024).
15. Schimmel, H., Kearley, G., Huot, J. & Mulder, F. Hydrogen diffusion in magnesium metal (alpha phase) studied by ab initio computer simulations. *J. Alloy. Compd.* **404–406**, 235–237, DOI: <https://doi.org/10.1016/j.jallcom.2004.11.100> (2005). Proceedings of the 9th International Symposium on Metal-Hydrogen Systems, Fundamentals and Applications (MH2004).
16. Klyukin, K., Shelyapina, M. G. & Fruchart, D. Dft calculations of hydrogen diffusion and phase transformations in magnesium. *J. Alloy. Compd.* **644**, 371–377, DOI: <https://doi.org/10.1016/j.jallcom.2015.05.039> (2015).
17. Shelyapina, M. G. Hydrogen diffusion on, into and in magnesium probed by dft: A review. *Hydrogen* **3**, 285–302, DOI: [10.3390/hydrogen3030017](https://doi.org/10.3390/hydrogen3030017) (2022).
18. Nishimura, C., Komaki, M. & Amano, M. Hydrogen permeation through magnesium. *J. Alloy. Compd.* **293–295**, 329–333, DOI: [https://doi.org/10.1016/S0925-8388\(99\)00373-4](https://doi.org/10.1016/S0925-8388(99)00373-4) (1999).
19. Uchida, H. *et al.* Absorption kinetics and hydride formation in magnesium films: Effect of driving force revisited. *Acta Materialia* **85**, 279–289, DOI: <https://doi.org/10.1016/j.actamat.2014.11.031> (2015).
20. Renner, J. & Grabke, H. J. Bestimmung von diffusionskoeffizienten bei der hydrierung von legierungen. *Int. J. Mater. Res.* **69**, 639–642, DOI: [doi:10.1515/ijmr-1978-691005](https://doi.org/10.1515/ijmr-1978-691005) (1978).
21. Kwon, H., Shiga, M., Kimizuka, H. & Oda, T. Accurate description of hydrogen diffusivity in bcc metals using machine-learning moment tensor potentials and path-integral methods. *Acta Materialia* **247**, 118739, DOI: <https://doi.org/10.1016/j.actamat.2023.118739> (2023).
22. Tang, H. *et al.* Reinforcement learning-guided long-timescale simulation of hydrogen transport in metals. *Adv. Sci.* **11**, 2304122, DOI: <https://doi.org/10.1002/advs.202304122> (2024). <https://onlinelibrary.wiley.com/doi/pdf/10.1002/advs.202304122>.
23. Kimizuka, H., Thomsen, B. & Shiga, M. Artificial neural network-based path integral simulations of hydrogen isotope diffusion in palladium. *J. Physics: Energy* **4**, 034004, DOI: [10.1088/2515-7655/ac7e6b](https://doi.org/10.1088/2515-7655/ac7e6b) (2022).
24. Lu, G. M., Witman, M., Agarwal, S., Stavila, V. & Trinkle, D. R. Explainable machine learning for hydrogen diffusion in metals and random binary alloys. *Phys. Rev. Mater.* **7**, 105402, DOI: [10.1103/PhysRevMaterials.7.105402](https://doi.org/10.1103/PhysRevMaterials.7.105402) (2023).
25. Friederich, P., Häse, F., Proppe, J. & Aspuru-Guzik, A. Machine-learned potentials for next-generation matter simulations. *Nat. Mater.* **20**, 750–761, DOI: [10.1038/s41563-020-0777-6](https://doi.org/10.1038/s41563-020-0777-6) (2021).
26. Yu, F., Xiang, X., Zu, X. & Hu, S. Hydrogen diffusion in zirconium hydrides from on-the-fly machine learning molecular dynamics. *Int. J. Hydrog. Energy* **56**, 1057–1066, DOI: <https://doi.org/10.1016/j.ijhydene.2023.12.241> (2024).
27. Vandenhoute, S., Cools-Ceuppens, M., DeKeyser, S., Verstraelen, T. & Van Speybroeck, V. Machine learning potentials for metal-organic frameworks using an incremental learning approach. *npj Comput. Mater.* **9**, 1–8 (2023).
28. Kývala, L., Angeletti, A., Franchini, C. & Dellago, C. Diffusion and coalescence of phosphorene monovacancies studied using high-dimensional neural network potentials. *The J. Phys. Chem. C* **127**, 23743–23751, DOI: [10.1021/acs.jpcc.3c05713](https://doi.org/10.1021/acs.jpcc.3c05713) (2023). <https://doi.org/10.1021/acs.jpcc.3c05713>.
29. Wang, N. & Huang, S. Molecular dynamics study on magnesium hydride nanoclusters with machine-learning interatomic potential. *Phys. Rev. B* **102**, 094111, DOI: [10.1103/PhysRevB.102.094111](https://doi.org/10.1103/PhysRevB.102.094111) (2020).
30. Lu, G. M., Witman, M., Agarwal, S., Stavila, V. & Trinkle, D. R. Explainable machine learning for hydrogen diffusion in metals and random binary alloys. *Phys. Rev. Mater.* **7**, 105402, DOI: [10.1103/PhysRevMaterials.7.105402](https://doi.org/10.1103/PhysRevMaterials.7.105402) (2023).
31. Deng, B., Zhong, P., Jun, K. *et al.* Chgnet as a pretrained universal neural network potential for charge-informed atomistic modelling. *Nat. Mach. Intell.* **5**, 1031–1041, DOI: [10.1038/s42256-023-00716-3](https://doi.org/10.1038/s42256-023-00716-3) (2023).
32. Batatia, I., Kovacs, D. P., Simm, G., Ortner, C. & Csanyi, G. Mace: Higher order equivariant message passing neural networks for fast and accurate force fields. In Koyejo, S. *et al.* (eds.) *Advances in Neural Information Processing Systems*, vol. 35, 11423–11436 (Curran Associates, Inc., 2022).
33. Jinnouchi, R., Karsai, F., Verdi, C., Asahi, R. & Kresse, G. Descriptors representing two- and three-body atomic distributions and their effects on the accuracy of machine-learned inter-atomic potentials. *The J. Chem. Phys.* **152**, 234102, DOI: [10.1063/5.0009491](https://doi.org/10.1063/5.0009491) (2020). https://pubs.aip.org/aip/jcp/article-pdf/doi/10.1063/5.0009491/15575269/234102_1_online.pdf.

34. Jinnouchi, R., Karsai, F. & Kresse, G. On-the-fly machine learning force field generation: Application to melting points. *Phys. Rev. B* **100**, 014105, DOI: [10.1103/PhysRevB.100.014105](https://doi.org/10.1103/PhysRevB.100.014105) (2019).
35. Kresse, G. & Furthmüller, J. Efficient iterative schemes for ab initio total-energy calculations using a plane-wave basis set. *Phys. Rev. B* **54**, 11169–11186, DOI: [10.1103/PhysRevB.54.11169](https://doi.org/10.1103/PhysRevB.54.11169) (1996).
36. Kresse, G. & Joubert, D. From ultrasoft pseudopotentials to the projector augmented-wave method. *Phys. Rev. B* **59**, 1758–1775, DOI: [10.1103/PhysRevB.59.1758](https://doi.org/10.1103/PhysRevB.59.1758) (1999).
37. Perdew, J. P., Burke, K. & Wang, Y. Generalized gradient approximation for the exchange-correlation hole of a many-electron system. *Phys. Rev. B* **54**, 16533–16539, DOI: [10.1103/PhysRevB.54.16533](https://doi.org/10.1103/PhysRevB.54.16533) (1996).
38. Riebesell, J. *et al.* Matbench discovery—an evaluation framework for machine learning crystal stability prediction. *arXiv preprint arXiv:2308.14920* (2023).
39. Batatia, I. *et al.* A foundation model for atomistic materials chemistry. *arXiv preprint* (2023). ArXiv:2401.00096 [physics.chem-ph].
40. Jain, A. *et al.* Commentary: The materials project: A materials genome approach to accelerating materials innovation. *APL materials* **1** (2013).
41. Thompson, A. P. *et al.* LAMMPS - a flexible simulation tool for particle-based materials modeling at the atomic, meso, and continuum scales. *Comp. Phys. Comm.* **271**, 108171, DOI: [10.1016/j.cpc.2021.108171](https://doi.org/10.1016/j.cpc.2021.108171) (2022).
42. Larsen, A. H. *et al.* The atomic simulation environment—a python library for working with atoms. *J. Physics: Condens. Matter* **29**, 273002, DOI: [10.1088/1361-648X/aa680e](https://doi.org/10.1088/1361-648X/aa680e) (2017).
43. Verdi, C., Ranalli, L., Franchini, C. & Kresse, G. Quantum paraelectricity and structural phase transitions in strontium titanate beyond density functional theory. *Phys. Rev. Mater.* **7**, L030801, DOI: [10.1103/PhysRevMaterials.7.L030801](https://doi.org/10.1103/PhysRevMaterials.7.L030801) (2023).
44. Ranalli, L. *et al.* Temperature-dependent anharmonic phonons in quantum paraelectric ktao3 by first principles and machine-learned force fields. *Adv. Quantum Technol.* **6**, 2200131, DOI: <https://doi.org/10.1002/qute.202200131> (2023). <https://onlinelibrary.wiley.com/doi/pdf/10.1002/qute.202200131>.
45. Verdi, C., Karsai, F., Liu, P., Jinnouchi, R. & Kresse, G. Thermal transport and phase transitions of zirconia by on-the-fly machine-learned interatomic potentials. *npj Comput. Mater.* **7**, 156 (2021).
46. Liu, P., Verdi, C., Karsai, F. & Kresse, G. Phase transitions of zirconia: Machine-learned force fields beyond density functional theory. *Phys. Rev. B* **105**, L060102, DOI: [10.1103/PhysRevB.105.L060102](https://doi.org/10.1103/PhysRevB.105.L060102) (2022).